

Transport coefficients for dense metal plasmas

Sandra Kuhlbrodt and Ronald Redmer

Universität Rostock, Fachbereich Physik, D-18051 Rostock, Germany

(Received 16 May 2000)

Thermoelectric transport coefficients of metal plasmas are calculated within the linear response theory applied previously to determine the electrical conductivity of Al and Cu plasmas [R. Redmer, Phys. Rev. E **59**, 1073 (1999)]. We consider temperatures of 1–3 eV and densities of 0.001–1 g/cm³ as relevant in rapid wire evaporation experiments. The plasma composition is calculated considering higher ionization stages of atoms up to 5+, and solving the respective system of coupled mass action laws. Interactions between charged particles are treated on T matrix level. Results for the electrical conductivity of various metal plasmas are in reasonable agreement with experimental data. Thermal conductivity and thermopower are also given. In addition, we compare with experimental data for temperatures up to 25 eV and liquidlike densities.

PACS number(s): 52.25.Fi, 52.25.Jm, 05.60.-k, 51.10.+y

I. INTRODUCTION

Transport coefficients are used to characterize the state of a plasma. For instance, varying density and temperature, metal-nonmetal transitions may occur in dense hydrogen [1] or expanded fluid metals [2] which can be observed via electrical conductivity. The energy balance of astrophysical objects depends strongly on the thermal conductivity, which has to be known for a large domain of densities and temperatures for stellar or planetary matter [3]. The efficiency of pulsed power machines designed to produce inertial confinement fusion plasmas [4] is mainly determined by the electrical conductivity of the exploding wire array and the thermal conductivity of the plasma. The reflectivity of plasmas generated by irradiation of ultrashort laser pulses on solid surfaces is governed by the optical conductivity [5].

Various methods of many-particle theory were applied to generalize the standard Spitzer theory [6], and to calculate transport coefficients for strongly coupled plasmas. Based on the Ziman formula [7], self-consistent calculations for the frequency and wave vector dependent dielectric function and the structure factors of fully ionized plasma were performed [8–10], or electron-ion pseudopotentials and ion-ion structure factors were determined [11]. Density functional theory was applied to calculate the conductivity from the weak-isolated-scatterer limit up to that of strong multiple scattering self-consistently with the equation of state [12]. Standard kinetic theory was also used to calculate the transport coefficients of strongly coupled plasmas [13,14].

In a previous paper [15] (hereafter denoted as I), we calculated the electrical conductivity of dense Al and Cu plasmas, applying linear response theory in the formulation of Zubarev [16]. This method allows one to evaluate the thermoelectric transport coefficients of electrical conductivity, thermal conductivity, and thermopower for arbitrary degeneracy, and reproduces the well-known Spitzer results for nondegenerate, weakly coupled plasmas as well as the Ziman theory for degenerate, strongly coupled plasmas [17,18]. Partial ionization of the plasma can be treated as well. The plasma composition was determined in I by considering ionization stages up to 3+, and solving the corresponding mass action laws. Scattering mechanisms between particles (elec-

trons, various ion species, atoms) were treated on a T matrix level. Reasonable agreement with electrical conductivities derived from experiments in which Al and Cu wires were evaporated rapidly from a solid state density ϱ_0 down to $0.001 \times \varrho_0$, by increasing the temperature from room temperature to about 1–3 eV [19,20], was achieved. In particular, the minimum of the electrical conductivity as a function of mass density observed experimentally for low temperatures can be explained by partial ionization.

New conductivity experiments were recently performed in the same parameter domain by DeSilva and Katsourous using Fe, Ni, and W wires [21], and by Haun and Kunze for Zn [22] and C [23]. Aluminum plasmas at much higher temperatures up to about 25 eV were generated in a tamped exploding wire z pinch [24]. Electrical conductivity in the solid, liquid, and plasma state was inferred from reflectivity measurements of thin aluminum layers embedded in a laser-heated target [25]. These data indicate a metal-insulator transition in the warm, expanded fluid around 0.5 eV and 1.7 g/cm³. However, new first-principles calculations show no evidence of such a transition [26].

It is the aim of the present paper (i) to generalize the method outlined in I, so that thermal conductivity and thermopower of dense metal plasmas can be determined in addition to the electrical conductivity; (ii) to calculate these transport coefficients for Al, Fe, Ni, Cu, Zn, and W plasma; and (iii) to compare with experimental data [20,21,23]. In addition, we study the high-temperature and high-density behavior of the electrical conductivity. Therefore, we consider a maximum ionization stage of 5+ instead of 3+ to determine the composition of the plasma and compare with the experimental data of Benage *et al.* [24].

This paper is organized as follows. The equation of state and plasma composition are calculated in Sec. II. We summarize the linear response theory for the transport coefficients in Sec. III, and demonstrate its capacity by comparing with electrical conductivities derived from the famous shock-wave experiments of Ivanov *et al.* for Ar and Xe [27]. Results for the transport coefficients of metal plasmas are given in Sec. IV for temperatures of 1–3 eV and for densities up to 1 g/cm³. In Sec. V, we apply the present theory to Al plasma for temperatures up to about 25 eV, and study the high-

TABLE I. Parameters for the evaluation of the coupled mass action laws according to Eq. (4), and atomic weight for the materials under consideration [28].

	Al	Fe	Ni	Cu	Zn	W	Ar	Xe
Z	13	26	28	29	30	74	18	54
$E_{\text{ion}}^{(1)}$ in eV	5.986	7.87	7.635	7.726	9.394	7.98	15.76	12.13
$E_{\text{ion}}^{(2)}$ in eV	18.829	16.18	18.168	20.293	17.964	17.81	27.629	21.21
$E_{\text{ion}}^{(3)}$ in eV	28.448	30.651	35.17	36.841	39.772	24.1	40.74	32.1
$E_{\text{ion}}^{(4)}$ in eV	119.99	54.8	54.9	55.2	59.4	35.4	59.81	
$E_{\text{ion}}^{(5)}$ in eV	153.71	75	75.5	79.9	82.6	48.0	75.02	
α_D in a_B^3	56.28	56.686	45.889	41.165	47.913	74.906	11.075	27.902
r_0 in a_B	1.861	1.759	1.658	1.609	1.666	1.728	1.206	1.386
atomic weight in u	26.982	55.847	58.70	63.546	65.38	183.5	39.948	131.29

density limit. In both Secs. IV and V, we compare with experimental data and give a short comparison with other theoretical approaches [9,11,14,29]. Conclusions and an outlook are given in Sec. VI.

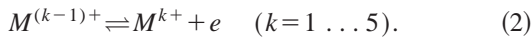
II. PLASMA COMPOSITION

Dense metal plasmas consist of electrons, atoms, and various ion species M^{k+} . In paper I we considered ions up to $k=3$, which is sufficient for temperatures of about 30 000 K. In order to treat higher temperatures up to 280 000 K, we generalized the model, and now consider a maximum charge state of $k=5$. The free electron density n_e and the total ion density n_i are then given by

$$n_e = \sum_{k=1}^5 kn_k, \quad n_i = \sum_{k=1}^5 n_k, \quad (1)$$

where n_k is the partial density of the k -fold ionized species M^{k+} . Besides the charged components, neutral atoms M^0 also may occur, especially for low temperatures, so that a partially ionized plasma (PIP) model applies.

The composition of such a multicomponent plasma is determined by the reactions between the various species, i.e., ionization processes up to M^{5+} :



The partial densities are derived from respective conditions of chemical equilibrium,

$$\mu_{k-1} = \mu_k + \mu_e + E_{\text{ion}}^{(k)} \quad (k=1 \dots 5). \quad (3)$$

The energies necessary for the excitation of the different ionization states M^{k+} are denoted by $E_{\text{ion}}^{(k)}$ and are given for the metals Al, Fe, Ni, Cu, Zn, and W in Table I. Parameters for Ar and Xe are shown in addition because we also apply our approach to the conditions reached in the shock-wave experiments of Ivanov *et al.* [27]. Following the method outlined in paper I, a system of coupled mass action laws is derived which determines the plasma composition for given temperatures and total mass densities according to

$$n_{k-1} = \frac{g_{k-1}n_k}{g_k} \exp[\beta(\mu_e^{\text{id}} + E_{\text{ion}}^{(k)} + \Delta\mu_k)]. \quad (4)$$

$\beta=1/(k_B T)$ is the inverse temperature, and g_k the spin factor of the ion. For metals with an odd atomic number, we have $g_0=2, g_1=1, g_2=2, g_3=1, \dots$, whereas for an even atomic number $g_0=1, g_1=2, g_2=1, g_3=2, \dots$ holds.

Accounting for an arbitrary degeneracy of the electrons, the ideal part of the chemical potential is determined by Fermi integrals of order 1/2,

$$F_{1/2}(\beta\mu_e^{\text{id}}) = \frac{n_e \Lambda_e^3}{2}, \quad (5)$$

where $\Lambda_e^2 = 2\pi\beta\hbar^2/m_e$ is the thermal wavelength.

The quantities $\Delta\mu_k = \mu_k^{\text{int}} - \mu_{k-1}^{\text{int}} + \mu_e^{\text{int}}$ are given by the interaction contributions to the chemical potentials, and yield a shift of the chemical equilibria compared with the ideal Saha equations. They can be interpreted as a lowering of the respective ionization energies $E_{\text{ion}}^{(k)}$ with increasing density, which leads to pressure ionization.

For contributions due to charged particle interactions, efficient Padé formulas were derived for fully ionized, two-component electron-ion plasmas that are applicable in a large domain of the density-temperature plane [30]. For the generalized case of a multicomponent plasma with various ionization states, similar expressions were given by Förster and co-worker [29,31].

In the case of partial ionization, a polarization contribution arises due to the interaction between electrons and neutral atoms. This term is usually parametrized as a linearized virial coefficient with respect to a screened polarization potential [32]; for details, see I.

The plasma composition is characterized by

$$\alpha_e = n_e/(n_0 + n_i), \quad \alpha_k = n_k/(n_0 + n_i). \quad (6)$$

The ionization degree α_e is the average number of free electrons generated per heavy particle, while α_k denotes the relative fraction of the ion species M^{k+} with respect to the total number of heavy particles. We show the results for the composition of Al plasma as a function of density for a constant temperature of 20 000 K in Fig. 1, and as a function of temperature for a constant density of 0.2 g/cm³ in Fig. 2, respectively.

While Al¹⁺ and Al²⁺ ions dominate at lower densities, neutral atoms occur with increasing density, and the ionization degree α_e decreases. Approaching solid state density,

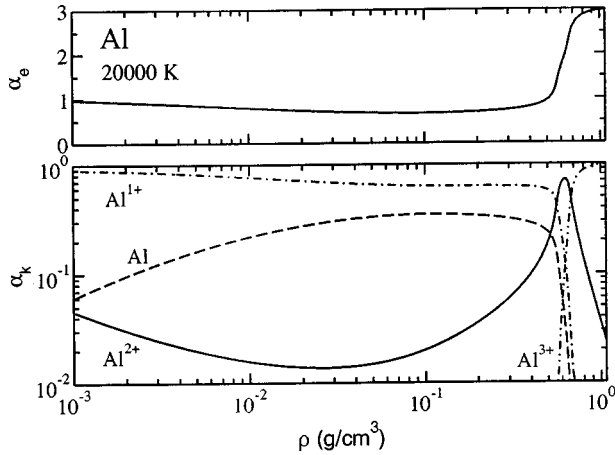


FIG. 1. Composition of Al plasma at 20 000 K according to Eq. (6). The upper panel shows the ionization degree α_e as function of mass density, and the lower panel the relative fraction α_k of Al^{k+} ions for the same densities.

Al^{3+} ions become important because of pressure ionization, and the ionization degree increases rapidly toward a value of 3; see Fig. 1. The minimum of the ionization degree is located at about 0.1 g/cm^3 . No ions with a higher charge than 3+ occur at relatively low temperatures of 1–3 eV; they are excited for temperatures above 10 eV (see Fig. 2). The composition of the other metals shows a similar behavior.

Electrical and thermal current are proportional to the number of free electrons n_e . We show this quantity as a function of mass density in Fig. 3 for all metals in the case of a constant temperature of 20 000 K. Especially at low densities $n_e^{\text{Fe}} \approx n_e^{\text{Ni}} \approx n_e^{\text{Cu}} \approx n_e^{\text{Zn}}$ because of the similar atomic properties; compare Table I. Aluminum despite a similar ionization degree α_e , has a higher free electron density n_e at the same mass density than these metals because of the lower atomic weight. For tungsten we find the opposite behavior because of the higher atomic weight.

Disregarding the influence of collisions, we can expect aluminum to have the best electrical and thermal conductivity of these metals at a given mass density and temperature for that reason. The behavior of the transport properties of iron, nickel, copper, and zinc should be very similar. Tung-

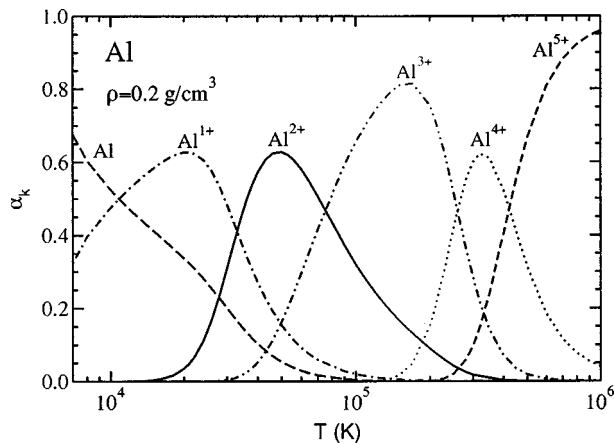


FIG. 2. Composition of Al plasma as a function of temperature for 0.2 g/cm^3 .

sten is expected to be the metal with the poorest electrical and thermal conductivity at a given mass density. The free electron density of aluminum increases more rapidly at high densities compared with the other metals, which is related to an earlier onset of pressure ionization.

III. TRANSPORT COEFFICIENTS

A. General expressions

The electrical conductivity σ , the thermopower κ , and the thermal conductivity λ are well known for nondegenerate, low-density plasmas where the Spitzer theory [6] applies. For strongly coupled, degenerate systems such as fluid metals, the Ziman theory is applicable [7]; the electrical conductivity is given by the Ziman formula, the thermal conductivity by the Wiedemann-Franz relation, and the thermopower by the Mott formula.

A general approach to the thermoelectric transport properties of Coulomb systems valid for arbitrary degeneracy was derived within linear response theory in the formulation of Zubarev [16]. Applying this correlation function method, the Onsager coefficients L_{ik} , that are connected to the transport coefficients σ , κ , and λ via

$$\sigma = e^2 L_{11},$$

$$\kappa = \frac{1}{eT} \frac{L_{12}}{L_{11}}, \quad (7)$$

$$\lambda = \frac{1}{T} \left(L_{22} - \frac{L_{12}L_{21}}{L_{11}} \right),$$

can be given in the standard determinant representation [17,18,33].

$$L_{ik} = - \frac{(-h)^{i+k-2}}{\Omega_0 |D|} \begin{vmatrix} 0 & \frac{k-1}{\beta h} Q_1 - Q_0 \\ \frac{i-1}{\beta h} N_1 - N_0 & D \end{vmatrix},$$

$$Q_m = (Q_{m0} Q_{m1} \dots Q_{mL}), \quad (8)$$

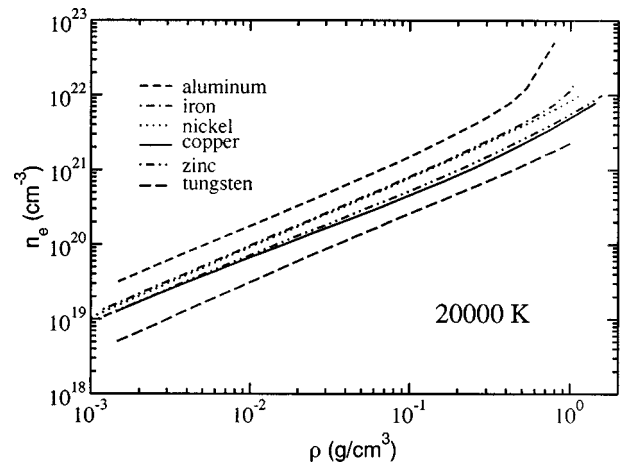


FIG. 3. Free electron density vs mass density for various metals at 20 000 K.

$$N_m = \begin{pmatrix} N_{0m} \\ N_{1m} \\ \vdots \\ N_{Lm} \end{pmatrix}, \quad D = \begin{pmatrix} D_{00} & D_{01} & \dots & D_{0L} \\ D_{10} & D_{11} & \dots & D_{1L} \\ \vdots & \vdots & \ddots & \vdots \\ D_{L0} & D_{L1} & \dots & D_{LL} \end{pmatrix}.$$

$h = \frac{5}{2}k_B T$ denotes the enthalpy per particle. The elements of the determinants are equilibrium correlation functions,

$$\begin{aligned} Q_{nm} &= N_{nm} + \frac{1}{m_e} \langle \mathbf{P}_n(\varepsilon); \dot{\mathbf{P}}_m \rangle, \\ N_{nm} &= \frac{1}{m_e} (\mathbf{P}_n, \mathbf{P}_m), \\ D_{nm} &= \langle \dot{\mathbf{P}}_n(\varepsilon); \dot{\mathbf{P}}_m \rangle, \\ \dot{\mathbf{P}}_n &= \frac{i}{\hbar} [H_S, \mathbf{P}_n], \end{aligned} \quad (9)$$

defined by Kubo scalar products and their Laplace transforms:

$$\begin{aligned} (A, B) &= \int_0^\beta d\tau \text{Tr} \{ \varrho_0 A(-i\hbar\tau) B \}, \\ \langle A(\varepsilon); B \rangle &= \lim_{\varepsilon \rightarrow 0} \int_{-\infty}^0 dt e^{\varepsilon t} (A(t), B), \\ A(t) &= e^{iH_S t/\hbar} A(0) e^{-iH_S t/\hbar}, \\ \varrho_0 &= \frac{1}{Z_0} \exp \left(-\beta H_S + \beta \sum_d \mu_d N_d \right). \end{aligned} \quad (10)$$

The system Hamiltonian H_S contains the kinetic energy of electrons, $E_e(k) = \hbar^2 k^2 / (2m_e)$, and their interactions with other electrons, atoms, and ions of species $d = \{1+, 2+, \dots, 5+\}$ via the potential $V(q)$ according to

$$\begin{aligned} H_S &= \sum_{\mathbf{k}} E_e(k) a_e^\dagger(\mathbf{k}) a_e(\mathbf{k}) + \sum_{\mathbf{p}, \mathbf{k}, \mathbf{q}} V_{ee}(q) a_e^\dagger(\mathbf{k} + \mathbf{q}) \\ &\times a_e^\dagger(\mathbf{p} - \mathbf{q}) a_e(\mathbf{p}) a_e(\mathbf{k}) + \sum_d \sum_{\mathbf{p}, \mathbf{k}, \mathbf{q}} V_{ed}(q) \\ &\times a_e^\dagger(\mathbf{k} + \mathbf{q}) a_d^\dagger(\mathbf{p} - \mathbf{q}) a_d(\mathbf{p}) a_e(\mathbf{k}). \end{aligned} \quad (11)$$

N_d and N_i are the numbers of ions d and the total number of ions, respectively.

The generalized moments \mathbf{P}_n of the electron system,

$$\mathbf{P}_n = \sum_{\mathbf{k}} \hbar \mathbf{k} [\beta E_e(k)]^n a_e^\dagger(\mathbf{k}) a_e(\mathbf{k}), \quad (12)$$

are a set of relevant observables which characterize the non-equilibrium state. The terms of lowest order are related to the total electron momentum (\mathbf{P}_0) and the ideal part of the electronic heat current (\mathbf{P}_1). They are connected with the microscopic expressions for the electrical current density and the electronic heat current density, respectively. A set of three

moments $\{n\} = \{0, 1, 2\}$, i.e., $L = 2$, is sufficient to determine the transport coefficients within 1.5% accuracy [33], see Sec. III C.

B. Evaluation of the correlation functions

Neglecting the terms $\langle \mathbf{P}_n(\varepsilon); \dot{\mathbf{P}}_m \rangle$ which are related to the Debye-Onsager relaxation effect, we have $Q_{nm} = N_{nm}$ in Eq. (9). The generalized particle numbers N_{nm} are given by Fermi integrals $F_n(x)$,

$$N_{nm} = N_e \frac{\Gamma(n+m+5/2)}{\Gamma(5/2)} \frac{F_{n+m+1/2}(\beta\mu_e^{\text{id}})}{F_{1/2}(\beta\mu_e^{\text{id}})}, \quad (13)$$

that are evaluated for given densities and temperatures.

The force-force correlation functions D_{nm} in Eq. (9) can be separated with respect to electron-electron, electron-ion, and electron-atom scattering [17, 18, 34]:

$$D_{nm} = D_{nm}^{ee} + D_{nm}^{ei} + D_{nm}^{ea}. \quad (14)$$

These terms can be evaluated within different approximations, related to the Landau, Lenard-Balescu, and Boltzmann collision integrals known from kinetic theory; see Ref. [18]. We will give results for the correlation functions within the Born and T matrix approximations.

The contributions D_{nm}^{ec} with $c = e, i, a$ are related to transport cross sections Q_T^{ec} , as shown for hydrogen plasma [17]. The electron-electron term reads

$$D_{nm}^{ee} = \frac{4}{3} \sqrt{\frac{2m_e}{\pi\beta}} n_e N_e \int_0^\infty dx x^3 R_{nm}(x) Q_T^{ee}(x) \exp(-x), \quad (15)$$

where $x = \beta \hbar^2 k^2 / m_e$. The polynomials R_{nm} can be found, for example, in Ref. [18].

The interaction of electrons with atoms and the different species of ions is presented by

$$\begin{aligned} D_{nm}^{ed} &= \frac{2\hbar}{3\pi^2} N_d \int_0^\infty dk k^3 [\beta E_e(k)]^{n+m+1} \\ &\times f_e(k) [1 - f_e(k)] Q_T^{ed}(k), \end{aligned} \quad (16)$$

with $d = \{a, +1, +2, +3, +4, +5\}$. The total electron-ion contribution D_{nm}^{ei} represents the weighted sum of the single contributions D_{nm}^{ek} :

$$D_{nm}^{ei} = \left| \sum_k \frac{N_k}{N_i} \sqrt{D_{nm}^{ek}} \right|^2. \quad (17)$$

N_e , N_i , and N_a are the electron, total ion, and atom particle numbers; N_k is the number of ions with charge $k+$.

In the T matrix approximation, electron-ion and electron-electron transport cross sections are given by scattering phase shifts δ_l within a partial wave expansion with respect to angular momentum l according to

$$Q_T^{ek}(k) = \frac{4\pi}{k^2} \sum_{l=0}^\infty (l+1) \sin^2[\delta_l^{ed}(k) - \delta_{l+1}^{ed}(k)], \quad (18)$$

$$Q_T^{ee}(k) = \frac{4\pi}{k^2} \sum_{l=0}^{\infty} \frac{(l+1)(l+2)}{2l+3} \left(1 - \frac{(-1)^l}{2}\right) \times \sin^2[\delta_l^{ee}(k) - \delta_{l+2}^{ee}(k)].$$

The scattering phase shifts are determined by a numerical solution of the Schrödinger equation with respect to the Debye potential,

$$V_{ed}^D(r) = -\frac{Z_d e^2}{4\pi\epsilon_0 r} \exp(-\kappa r), \quad (19)$$

where $Z_d = \{-1, +1, +2, \dots, +5\}$ is the charge of species $d = e, i$.

The electron-atom correlation function is evaluated in the Born approximation with respect to a polarization potential [32],

$$V_{ed}^{PP}(r) = -\frac{e^2 \alpha_D}{2(4\pi\epsilon_0)^2 (r^2 + r_0^2)^2}, \quad (20)$$

where the dipole polarizability α_D and the cutoff radius $r_0^4 = \alpha_D a_B / 2Z^{1/3}$ [35] are given in Table I for the materials under consideration. The inverse screening length κ is defined for arbitrary degeneracy by Fermi integrals of order $-1/2$ according to

$$\kappa^2 = \frac{\beta e^2}{\epsilon_0} \frac{2}{\Lambda_e^3} F_{-1/2}(\beta \mu_e^{\text{id}}), \quad (21)$$

reproducing the Debye screening length in the classical limit and the Thomas-Fermi screening length in the degenerate domain.

C. Model calculations

In order to demonstrate the convergence of the present linear response method, to study the influence of electron-electron scattering, and to verify the validity region of the Born approximation, we have performed model calculations for fully ionized hydrogen plasma as a reference system. There we can neglect the influence of neutral atoms and of higher charged ions. The electron-electron and electron-proton correlation functions [Eq. (15) and (17)] were calculated on a T matrix level; see Eq. (18).

Figure 4 shows the electrical conductivity as a function of electron density for a temperature of 10 000 K. A fast convergence of the presented method with respect to a systematic extension of the set of relevant observables $\{\mathbf{P}_n\}$ [Eq. (12)] can be seen. The use of three moments $\{\mathbf{P}_0, \mathbf{P}_1, \mathbf{P}_2\}$ is sufficient in all cases; these results are identical to the two-moment ones in this presentation. With increasing density, even fewer moments are needed to reach convergence. For instance, a one-moment approximation (taking only \mathbf{P}_0) is applicable above $3 \times 10^{21} \text{ cm}^{-3}$.

The Spitzer curve is reproduced in the low-density limit, evaluating the correlation functions D_{nm} on a T matrix level (see Refs. [18,36]), and we obtain

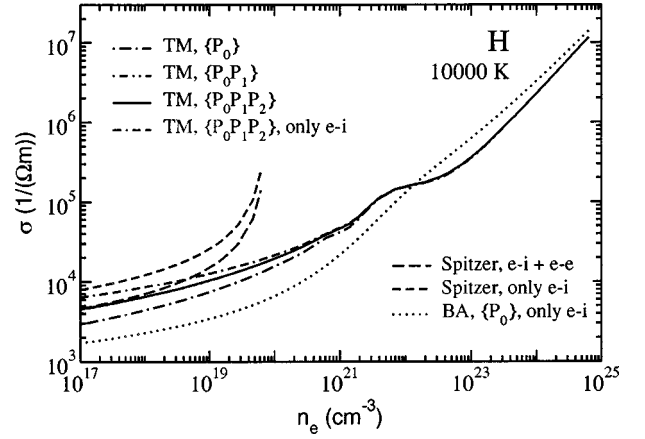


FIG. 4. Electrical conductivity of fully ionized hydrogen plasma as function of electron density for 10 000 K within the T matrix approximation (TM) using one, two, and three moments $\{\mathbf{P}_n\}$. For comparison, the conductivity for the Lorentz plasma model neglecting electron-electron scattering, the Spitzer curves including and neglecting electron-electron scattering, and the Born approximation (BA) using only one moment $\{\mathbf{P}_0\}$ for the Lorentz plasma model, are shown.

$$\sigma_{\text{Sp}} = \frac{0.591}{0.5 \ln(1.5 \Gamma^{-3})} \frac{(4\pi\epsilon_0)^2 (k_B T)^{3/2}}{e^2 m_e^{1/2}}. \quad (22)$$

$\Gamma = e^2 / (4\pi\epsilon_0 k_B T d)$ is the coupling parameter with the mean distance between ions $d = [3/(4\pi n_e)]^{1/3}$.

Electron-electron scattering is neglected in the Lorentz plasma model. The respective conductivity is too high by a factor of about 1.7 in the low-density limit. The Spitzer curve for the Lorentz plasma is also shown. The influence of electron-electron scattering is reduced with increasing density, and vanishes for densities above 10^{21} cm^{-3} .

The evaluation of correlation functions (15) and (17) within the T matrix approximation is important for lower densities where strong collisions have to be treated. On the other hand, the T matrix results merge into the Born approximation with respect to the Debye potential [Eq. (19)] in the high-density limit. There, strong screening effects lead to a weak interaction potential, so that the Born approximation becomes valid. Thus the well-known Ziman formula for the electrical conductivity,

$$\sigma_{\text{Zi}}^{-1} = \frac{\Omega_0 m_e^2 N_i}{12 \pi^2 \hbar^3 e^2 n_e^2} \int_0^\infty dq q^3 f(q/2) S_{ii}(q) \left| \frac{w_{ei}(q)}{\epsilon(q)} \right|^2, \quad (23)$$

can be derived in the present approach in the high-density limit within a one-moment solution of Eqs. (8), and evaluating electron-ion correlation function (17) in the Born approximation; see Ref. [37].

Instead of the Debye potential, a weak electron-ion pseudopotential $w_{ei}(q)$, which is screened by the dielectric function $\epsilon(q)$ has to be used for metal plasmas, including the static ion-ion structure factor $S_{ii}(q)$. $f(q/2)$ is the Fermi-Dirac distribution function. We conclude that the present approach to the transport coefficients is applicable for arbitrary

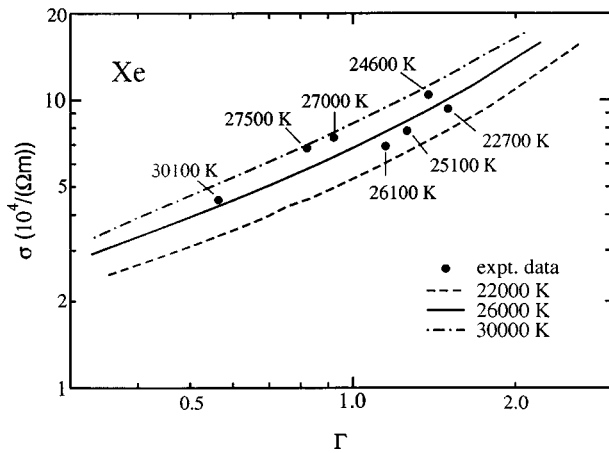


FIG. 5. Electrical conductivity of Xe plasma vs coupling parameter Γ . Theoretical curves for three typical temperatures are compared with experimental points [27].

degeneracy, interpolating between the Spitzer and Ziman theory for the low- and high-density limits; for details, see Refs. [17,18].

IV. RESULTS FOR THE ELECTRICAL CONDUCTIVITY

A. Rare gases

In order to check our approach, we first calculate the electrical conductivity for conditions reached in the famous shock wave experiments of Ivanov *et al.* [27]. They determined the Coulomb part of the measured conductivities by correcting the influence of the neutral particles (ionization degree, electron-atom transport cross sections). Therefore, we have taken their plasma parameters as input, derived the composition within the PIP model, and neglected electron-atom scattering. We compare these results as a function of coupling parameter Γ in Figs. 5 and 6, respectively.

A comparison between theoretical and experimental conductivities is always sensitive with respect to the equation of state data (density, temperature), which also affect the Coulomb logarithm via the ionization equilibrium; also see Rogers, DeWitt, and Boercker [13]. Keeping in mind both possible systematic and experimental errors in temperature and density measurements, the agreement between the data is

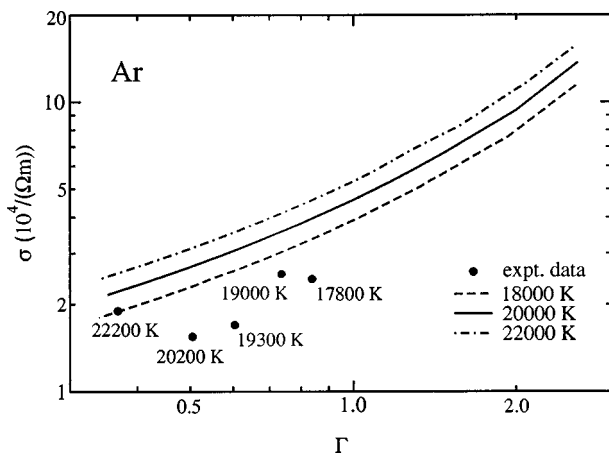


FIG. 6. Same as Fig. 5, but for Ar plasma.

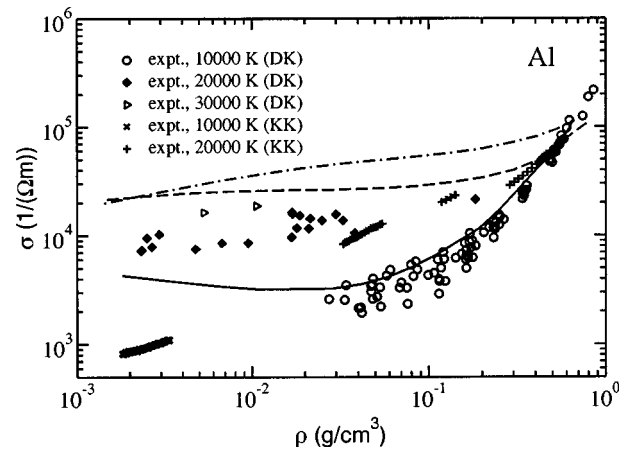


FIG. 7. Electrical conductivity of aluminum plasma. Theoretical results for 10 000 K (solid line), 20 000 K (dashed line), and 30 000 K (dot-dashed line) are compared with experimental points of DeSilva and Katsouros (DK) [19] and Krisch and Kunze (KK) [20].

good, especially for xenon. For argon, the theoretical curves are consistently higher than the experimental points.

B. Metal plasmas

DeSilva and Katsouros measured the electrical conductivity of aluminum, iron, nickel, copper, and tungsten via rapid wire vaporization in a water bath [19,21]. Kunze and co-workers performed similar experiments for aluminum [20], zinc [22], and carbon [23]. The same technique was used to measure conductivities in liquid zinc and tungsten close to the critical point [38], i.e., at lower temperatures as considered here. While in the shock wave experiments [27] maximum coupling parameters of $\Gamma \leq 1.5$ have been reached, the rapid wire evaporation technique is capable of producing strongly coupled plasmas up to $\Gamma \approx 200$.

Experimental data of DeSilva and Katsouros are compared in Figs. 7–11 with the present theoretical results for three typical plasma temperatures of 10 000, 20 000, and 30 000 K. For all metals, the electrical conductivity approaches the Spitzer values at low densities, passes through a minimum for $T \approx 10^4$ K around $\rho \approx 0.1$ g/cm³, and shows a subsequent sharp increase which is a direct result of the in-

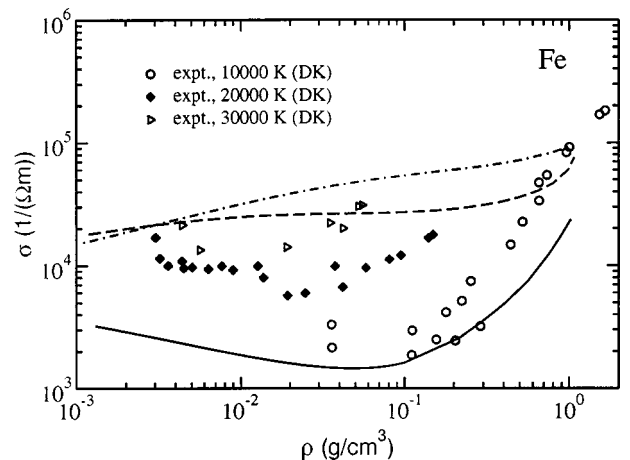


FIG. 8. Same as Fig. 7, but for iron with experimental points of DeSilva and Katsouros [21].

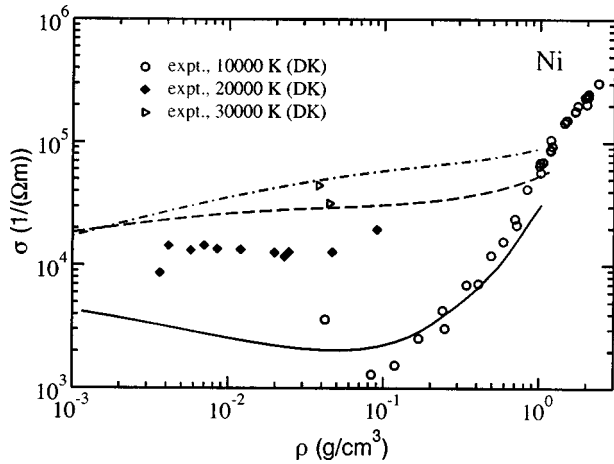


FIG. 9. Same as Fig. 7, but for nickel with experimental points of DeSilva and Katsouros [21].

creasing ionization degree; see Fig. 1.

The minimum behavior at low temperatures can be explained by the occurrence of neutral atoms. Starting at low densities, the relative fraction of free electrons is reduced, and their mobility decreases due to additional scattering processes at atoms. At high densities, the lowering of the ionization energies inverts this trend, and leads to a drastic increase of the ionization state which is known as pressure ionization. This typical behavior can be interpreted as a nonmetal-to-metal transition. Taking the Mott criterion [39] for the minimum metallic conductivity at $T=0$ K and $\sigma_{\min} \approx 10^4 (\Omega \text{ m})^{-1}$, for finite temperatures, in order to locate this electronic transition, a critical density of about $\rho_{\text{cr}} \approx 0.5 \text{ g/cm}^3$ is also found for all metals considered here.

Although the concepts applied for calculations of the plasma composition (coupled mass action laws) and the interactions between charged particles (Debye potential) are relatively simple, we can state a good overall agreement with the experimental data. Note that the results for copper have changed compared to I because we have removed an error in scaling the mass density. Using the Born approximation instead of the T matrix approximation for evaluating the

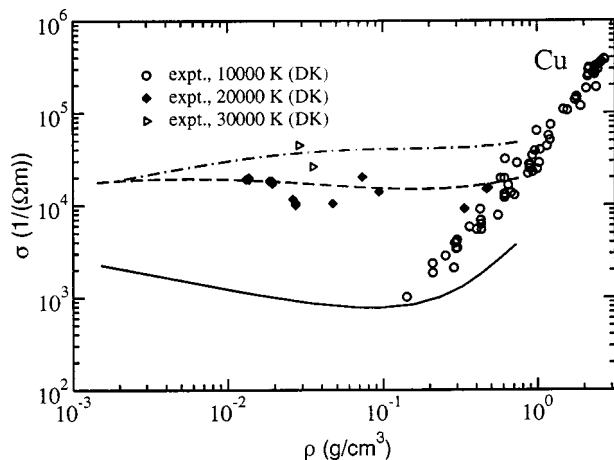


FIG. 10. Same as Fig. 7, but for copper with experimental points of DeSilva and Katsouros [19]. Note that the curves have changed compared to paper I.

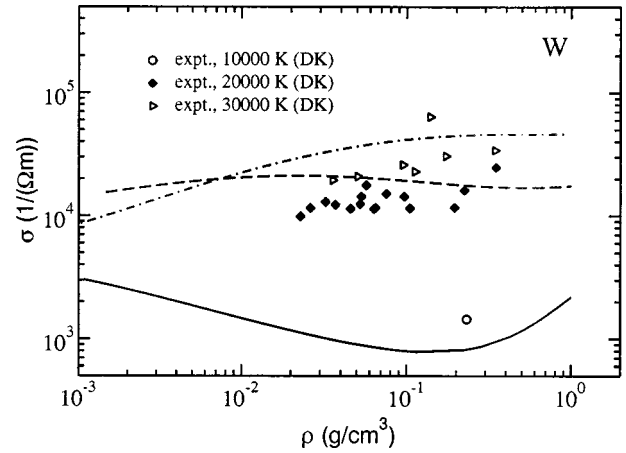


FIG. 11. Same as Fig. 7, but for tungsten with experimental points of DeSilva and Katsouros [21].

electron-atom transport cross section has almost no influence on the results.

Comparison with experimental data for zinc [23] is performed in Fig. 12. The measured conductivities are consistently higher than the theoretical ones. Kunze and co-workers determined the temperature spectroscopically instead of using equation of state data like DeSilva and Katsouros. This may be the source of systematic deviations; a more refined comparison of experimental data and standard equations of state is needed. However, we can again state agreement with trends of the conductivity as function of density and temperature, as found experimentally.

In paper I, a comparison with other theoretical results was shown for the electrical conductivity of aluminum at 10 000 and 20 000 K (Figs. 8 and 9). If we compare the results for the other metals with the same theoretical approaches, we obtain a similar behavior: The theory of Lee and More [14] is based on the relaxation time approximation for the solution of a Boltzmann transport equation valid for arbitrary degeneracy, but neglects electron-electron scattering. This theory yields an upper estimate for the plasma conductivity, and lies above our results. Rinker's theory [11] is based on the Ziman formula, which is applicable in the high-density region; see Fig. 4. The ion-ion structure factor and the effec-

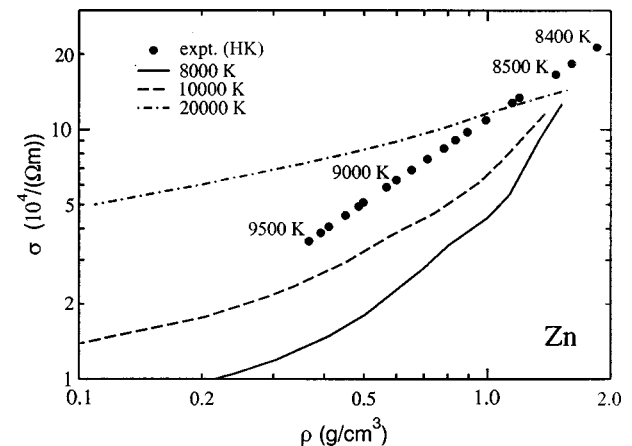


FIG. 12. Electrical conductivity of zinc plasma. Theoretical results for three temperatures are compared with experimental points of Haun and Kunze (HK) [22].

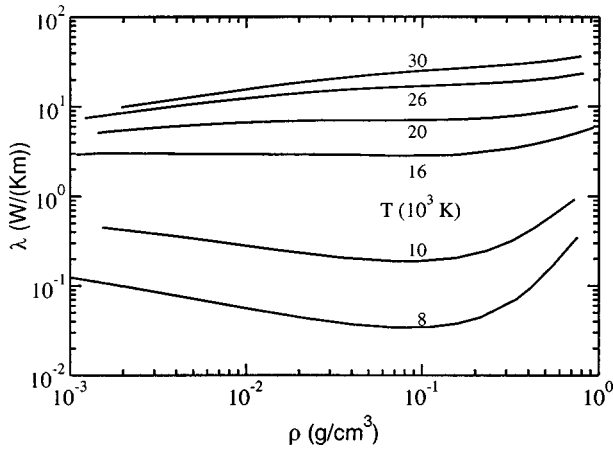


FIG. 13. Thermal conductivity of copper plasma for various temperatures.

tive electron-ion potential are determined self-consistently for various materials. This theory gives a lower estimate for the conductivity in the expanded fluid domain, as considered here. For increasing temperatures, the agreement between the different theories is improving especially with theoretical data based on a fully ionized plasma [9,29].

V. THERMAL CONDUCTIVITY OF METAL PLASMAS

In Fig. 13 we show the thermal conductivity λ of copper plasma as an example. The behavior is very similar to that of the electrical conductivity. The Spitzer value is recovered in the low-density limit. For low temperatures $T \leq 10\,000$ K, the thermal conductivity passes through a minimum with increasing density, and rises according to the Wiedemann-Franz relation at higher densities. The Lorentz number L , defined by

$$\lambda = L\sigma T \left(\frac{k_B}{e} \right)^2, \quad (24)$$

varies between 1.6 and 3.29 from the low- to high-density regions of a hydrogen plasma; see Ref. [18]. The metal plasmas follow this trend in the density region considered here. The thermal conductivity of the various metals is shown in Fig. 14 for a typical temperature of 20 000 K. As expected,

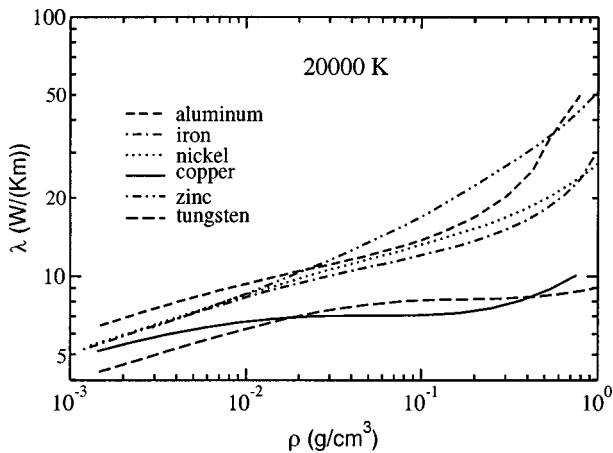


FIG. 14. Thermal conductivity of various metals at 20 000 K.

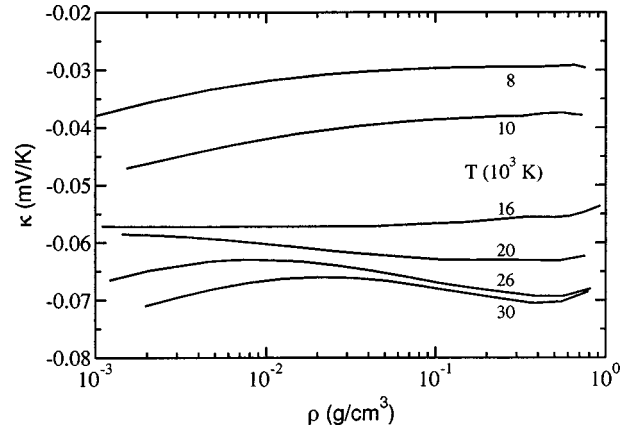


FIG. 15. Thermopower of copper plasma for various temperatures.

the thermal conductivities of copper, nickel, and iron are very similar in the low density limit due to similar atomic properties; see Table I. The thermal conductivity of tungsten is lower, and the one of aluminum higher, than the one of copper, which is a result of the differences in the electron density; see Fig. 3.

VI. THERMOPOWER OF METAL PLASMAS

The thermopower κ is a cross effect which describes the relation between the electrical and thermal current. It is defined as the electrical field strength created by a temperature gradient in the system for zero electrical current. The thermopower of metals is usually negative, characterized by the charge of the electrons.

In Fig. 15 we show the thermopower of copper plasma for various temperatures as an example. The behavior is very systematic. For lower temperatures the thermopower reaches higher values due to partial ionization, but is still negative. The thermopower of the metals under consideration is shown in Fig. 16 for 20 000 K. For low densities, a Spitzer value of -0.06 mV/K is reached. For high densities, it tends to zero according to the Mott formula.

The curve for aluminum rises very sharply for the highest densities considered, tending to positive values $\kappa > 0$. This interesting behavior is connected with the metal-to-nonmetal

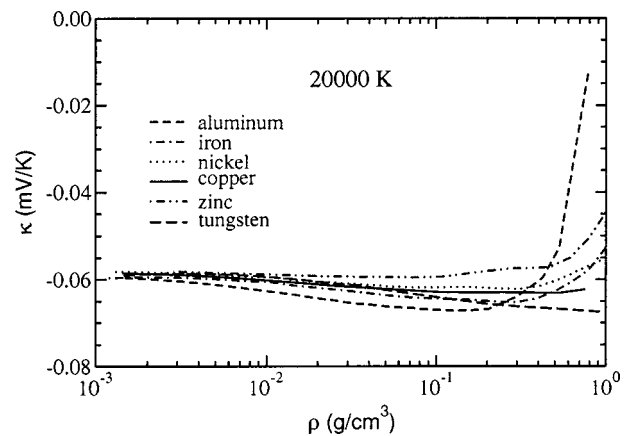


FIG. 16. Thermopower of various metals at 20 000 K.

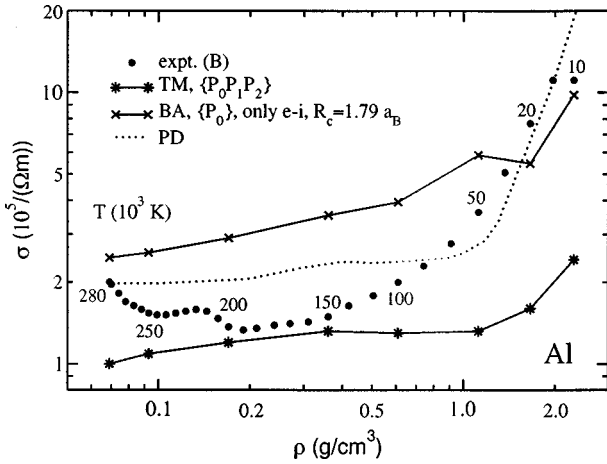


FIG. 17. Electrical conductivity of aluminum plasma as function of mass density. Filled circles represent experimental data of Benage *et al.* (B) [24]; some temperatures are indicated. The conductivity is calculated at the same densities and temperatures in T matrix approximation (TM) with respect to the Debye potential, and in Born approximation (BA) with respect to the Ashcroft empty-core potential (see the text). Theoretical results of Perrot and Dharma-Wardana (PD) are also given (dotted line) [12].

transition, which has been obtained for the electrical conductivity; see Figs. 7–11.

Such a metal-to-nonmetal transition is observed when expanding fluid metals like mercury or the alkali metals thermally from the melting point toward the critical point of the liquid-vapor phase transition. The simultaneous occurrence of a thermodynamic phase transition and an electronic transition gives rise to peculiarities in the physical properties, see Ref. [40]. For instance, experiments for expanded fluid mercury have shown that the thermopower can reach positive values near a critical temperature of $T_c = 1751$ K, and that the zero of the thermopower just coincides with the critical density of the liquid-vapor phase transition at $\rho_c = 5.80$ g/cm³ [41]. Therefore, a tendency of the thermopower toward positive values could be a hint for the existence of a phase transition or, at least, for an electronic transition.

VII. ELECTRICAL CONDUCTIVITY FOR HIGH TEMPERATURES AND DENSITIES

Benage *et al.* [24] measured the electrical conductivity of aluminum in an exploding wire z pinch. In these experiments, the initial density is about 3 g/cm³, and the initial temperature about 10 000 K. The density decreases due to thermal expansion to about 8×10^{-3} g/cm³, while the temperature increases up to 280 000 K. Therefore, these experiments are suitable to study the behavior of our method in the high-density and high-temperature limit. The T matrix approximation applied so far for the calculation of transport cross sections for charged particle scattering is in good agreement with the experimental data for temperatures above 100 000 K and below densities of 0.6 g/cm³ (see Fig. 17). The strong increase of the conductivity for lower temperatures and near-liquid-like densities cannot be reproduced. In this density region the Debye potential becomes an invalid approximation for the interaction potential between charged

particles. There a Born approximation with respect to a weak electron-ion pseudopotential should be applied; see Fig. 4.

In order to give a rough estimate for the effect of such a weak electron-ion pseudopotential on the conductivities, we utilize the Ashcroft empty-core potential [42] with a cutoff radius $R_c = 1.79 a_B$ for the evaluation of Eq. (23). This parameter is derived for the s -wave contribution ($l=0$) to the self-consistent Troullier-Martins pseudopotential for solid aluminum used in band structure calculations [43]. The dielectric function $\epsilon(q)$ was treated in the random phase approximation, with local-field corrections given by Ichimaru and Utsumi [44]. For simplicity, the ion-ion structure factor was neglected, i.e., $S_{ii}(q) = 1$. The evaluation of Eq. (23) on this simplest level gives substantially higher conductivities compared with the T matrix calculation, and the agreement with the experiments is incrementally improved for liquid-like densities.

The best agreement with the experimental data was achieved within density functional theory by Perrot and Dharma-Wardana [12], where the equation of state, a density-dependent electron-ion pseudopotential, and the ion-ion structure factor are determined self-consistently. The derivation of a density-dependent electron-ion potential which changes from a weak pseudopotential at high densities to a Debye-like potential for lower densities is needed. This is the aim of future work.

VIII. CONCLUSIONS

In this paper we have determined the electrical and thermal conductivity as well as the thermopower for aluminum, iron, nickel, copper, zinc, and tungsten plasmas within a partially ionized plasma model, originally developed for hydrogen plasma [17]. We have considered a realistic plasma composition. Interactions of free electrons with other electrons and the relevant ion species were treated on a T matrix level, and electron-atom scattering in the Born approximation.

The agreement with available experimental data for the electrical conductivity [19,20,22] is reasonable. The general behavior of expanded metal plasmas as a function of density and temperature can be understood within the present PIP model. In particular the metal-to-nonmetal transition in the expanded, partially ionized vapor can be explained by the occurrence of neutral atoms. This was already shown for expanded metal fluids such as cesium at lower temperatures [37]. The minimum behavior of the electrical conductivity, as found experimentally for low temperatures, can be reproduced.

Various improvements of the present approach are possible. For instance, the influence of non-Coulombic contributions to the electron-ion potentials has to be studied using self-consistent pseudopotentials rather than the Debye potential. A density-dependent electron-ion potential which changes from a weak pseudopotential at high densities to a Debye-like potential for lower densities has to be used. Furthermore, higher charged states beyond $k=5+$ may have an influence on the plasma properties at the highest densities and temperatures considered here. There the equation of state has to be improved. For high densities, structure factor effects and dynamic screening including local-field corrections also become of importance. In conclusion, the aim of future

work is the calculation of transport coefficients not only in the expanded plasma domain, but also for plasmas near and above liquidlike densities.

ACKNOWLEDGMENTS

We thank M. Desjarlais and T. Mehlhorn (Sandia), M. W. C. Dharma-Wardana (Ottawa), V. E. Fortov (Moscow), G. Röpke (Rostock), and S. Kosse and M. Schlanges (Greif-

swald) for helpful discussions and comments. We are indebted to A. W. DeSilva (College Park), J. Haun and H.-J. Kunze (Bochum), and J. Benage (Los Alamos) for sending us their experimental data for the electrical conductivity. We thank N. Fitzer (Rostock) for providing us with the self-consistent Troullier-Martins pseudopotential for solid aluminum and the respective Ashcroft empty-core radius. This study was supported by the Deutsche Forschungsgemeinschaft within the Sonderforschungsbereich 198 *Kinetics of Partially Ionized Plasmas*.

-
- [1] S.T. Weir, A.C. Mitchell, and W.J. Nellis, *Phys. Rev. Lett.* **76**, 1860 (1996); W.J. Nellis, S.T. Weir, and A.C. Mitchell, *Phys. Rev. B* **59**, 3434 (1999).
- [2] F. Hensel, *J. Phys.: Condens. Matter* **2**, 33 (1990).
- [3] E. Flowers and N. Itoh, *Astrophys. J.* **206**, 218 (1976); N. Itoh, S. Mitake, H. Iyetomi, and S. Ichimaru, *ibid.* **273**, 774 (1983).
- [4] R.B. Spielman *et al.*, *Phys. Plasmas* **5**, 2105 (1998).
- [5] H.M. Milchberg, R.R. Freeman, S.C. Davey, and R.M. More, *Phys. Rev. Lett.* **61**, 2364 (1988); D.F. Price *et al.*, *ibid.* **75**, 252 (1995); W. Theobald, R. Häßner, C. Wülker, and R. Sauerbrey, *ibid.* **77**, 298 (1996).
- [6] L. Spitzer, Jr., and R. Härm, *Phys. Rev.* **89**, 977 (1953).
- [7] J.M. Ziman, *Philos. Mag.* **6**, 1013 (1961).
- [8] S. Ichimaru and S. Tanaka, *Phys. Rev. A* **32**, 1790 (1985).
- [9] Z. Djurić, A.A. Mihajlov, V.A. Nastasyuk, M.M. Popović, and I.M. Tkachenko, *Phys. Lett. A* **155**, 415 (1991); see also V.M. Adamyán, Z. Djurić, A.M. Ermolaev, A.A. Mihajlov, and I.M. Tkachenko, *J. Phys. D* **27**, 111 (1994); **27**, 927 (1994).
- [10] I.M. Tkachenko and P. Fernández de Córdoba, *Phys. Rev. E* **57**, 2222 (1998).
- [11] G.A. Rinker, *Phys. Rev. B* **31**, 4207 (1985); **31**, 4220 (1985); *Phys. Rev. A* **37**, 1284 (1988).
- [12] F. Perrot and M.W.C. Dharma-Wardana, *Phys. Rev. B* **36**, 238 (1987); *Phys. Rev. E* **52**, 5352 (1995); M.W.C. Dharma-Wardana and F. Perrot, *ibid.* **58**, 3705 (1998).
- [13] D.B. Boercker, F.J. Rogers, and H.E. DeWitt, *Phys. Rev. A* **25**, 1623 (1982); see also D.B. Boercker, *ibid.* **23**, 1969 (1981); F.J. Rogers, H.E. DeWitt, and D.B. Boercker, *Phys. Lett. A* **82**, 331 (1981).
- [14] Y.T. Lee and R.M. More, *Phys. Fluids* **27**, 1273 (1984).
- [15] R. Redmer, *Phys. Rev. E* **59**, 1073 (1999).
- [16] D. N. Zubarev, *Nonequilibrium Statistical Thermodynamics* (Consultants Bureau, New York, 1974).
- [17] H. Reinholz, R. Redmer, and S. Nagel, *Phys. Rev. E* **52**, 5368 (1995).
- [18] R. Redmer, *Phys. Rep.* **282**, 35 (1997).
- [19] A.W. DeSilva and J.D. Katsouras, *Phys. Rev. E* **57**, 5945 (1998).
- [20] I. Krisch and H.-J. Kunze, *Phys. Rev. E* **58**, 6557 (1998).
- [21] A.W. DeSilva and J.D. Katsouras, *J. Phys. IV* **10**, 209 (2000).
- [22] J. Haun and H.-J. Kunze (private communication).
- [23] J. Haun and H.-J. Kunze, *Contrib. Plasma Phys.* **39**, 169 (1999).
- [24] J.F. Benage, Jr., W.R. Shanahan, and M.S. Murillo, *Phys. Rev. Lett.* **83**, 2953 (1999); J.F. Benage, Jr., *Phys. Plasmas* **7**, 2040 (2000).
- [25] A.N. Mostovych and Y. Chan, *Phys. Rev. Lett.* **79**, 5094 (1997).
- [26] P.L. Silvestrelli, *Phys. Rev. B* **60**, 16 382 (1999).
- [27] Yu.L. Ivanov, V.B. Mintsev, V.E. Fortov, and A.N. Dremin, *Zh. Éksp. Teor. Fiz.* **71**, 216 (1976) [*Sov. Phys. JETP* **44**, 112 (1976)].
- [28] *Handbook of Chemistry and Physics*, 1st student ed., edited by R. C. Weast (CRC Press, Boca Raton, FL, 1991).
- [29] W. Ebeling, A. Förster, V.E. Fortov, V.K. Gryaznov, and A. Ya. Polishchuk, *Thermophysical Properties of Hot Dense Plasmas* (Teubner Verlagsgesellschaft, Stuttgart-Leipzig, 1991), p. 39.
- [30] W. Ebeling and W. Richert, *Ann. Phys. (Leipzig)* **39**, 362 (1982); *Phys. Status Solidi B* **128**, 467 (1985); *Phys. Lett. A* **108**, 80 (1985); *Contrib. Plasma Phys.* **25**, 1 (1985).
- [31] A. Förster, Ph.D. thesis, Humboldt-Universität zu Berlin, 1991.
- [32] R. Redmer, G. Röpke, and R. Zimmermann, *J. Phys. B* **20**, 4069 (1987); R. Redmer, T. Rother, K. Schmidt, W.D. Kraeft, and G. Röpke, *Contrib. Plasma Phys.* **28**, 41 (1988).
- [33] H. Reinholz, R. Redmer, and D. Tamme, *Contrib. Plasma Phys.* **29**, 395 (1989).
- [34] F.E. Höhne, R. Redmer, G. Röpke, and H. Wegener, *Physica A* **128**, 643 (1984).
- [35] M.H. Mittleman and K.M. Watson, *Phys. Rev.* **113**, 198 (1959).
- [36] F. Sigeneger, S. Arndt, R. Redmer, M. Luft, D. Tamme, W.D. Kraeft, G. Röpke, and T. Meyer, *Physica A* **152**, 365 (1988).
- [37] R. Redmer, H. Reinholz, G. Röpke, R. Winter, F. Noll, and F. Hensel, *J. Phys.: Condens. Matter* **4**, 1659 (1992).
- [38] A. Kloss, T. Motzke, R. Grossjohann, and H. Hess, *Phys. Rev. E* **54**, 5851 (1996); A. Kloss, H. Hess, and H. Schneidenbach, *High Temp.-High Press.* **29**, 215 (1997).
- [39] N. F. Mott, *Conduction in Non-Crystalline Materials*, 2nd ed. (Oxford University Press, Oxford, 1993).
- [40] F. Hensel and W. W. Warren, Jr., *Fluid Metals* (Princeton University Press, Princeton, 1999).
- [41] W. Götzlaff, G. Schönherr, and F. Hensel, *Z. Phys. Chem. Neue Folge* **156-158**, 219 (1988).
- [42] N.W. Ashcroft, *Phys. Lett.* **23**, 48 (1966).
- [43] N. Troullier and J.L. Martins, *Phys. Rev. B* **43**, 1993 (1991).
- [44] S. Ichimaru and K. Utsumi, *Phys. Rev. B* **24**, 7385 (1981); see also K. Utsumi and S. Ichimaru, *ibid.* **22**, 1522 (1980); **22**, 5203 (1980).